A Plumber's View of Perturbative QCD*

J. D. BJORKEN

Stanford Linear Accelerator Center

Stanford University, Stanford, California 94309

ABSTRACT

The fractal phase space introduced by the Lund group for the description of QCD multijet phenomena is discussed using a different choice of coordinates. We advocate these coordinates as a useful diagnostic tool in the analysis of complex event structures. Features of QCD such as color-coherence or "angular ordering," and the "string effect," are described in this language.

Submitted to *Physical Review D.*

---

1. Introduction

The so-called lego plot, introduced to the best of my knowledge by some anonymous hero within the UA1 collaboration, has taken its place as an important diagnostic tool in contemporary particle physics. This occurs because for many purposes the most convenient variables to describe particle, parton, or jet coordinates are the rapidity y (or pseudo-rapidity η), azimuthal angle ϕ relative to the collision axis (or, in e^+e^- applications, the thrust axis), and magnitude of the momentum transverse to that axis, p_t. The reasons for this choice include the following:

1. Invariant phase-space is simply described with this choice:

$$\frac{d^3p}{E} = p_t dp_t dy \, d\phi \ . \tag{1.1}$$

2. These variables have simple transformation properties under longitudinal Lorentz boosts

$$p_t \to p_t \qquad \phi \to \phi \qquad y \to y + \text{const} \ . \tag{1.2}$$

3. The populations of produced particles are, in the absence of QCD jets, distributed very uniformly in the variables y and ϕ, while they are rather sharply centered in p_t about the mean value $\langle p_t \rangle$.

It is especially this third feature that motivated much work [1] in the early 1970s on building an analogy between populations of produced particles in the $y - \phi$ plane with populations of particles in a 2-dimensional fluid. On average, uniform density is expected in each case and, to large extent, this has been found experimentally.

With the advent of QCD, this picture has changed somewhat. The emission of perturbative gluons by the partons participating in the underlying collision process leads to clustering in the lego plot, and on occasion to strong concentrations of p_t (jets) within small regions of y and ϕ.

In an interesting series of papers [2] , Gustafsson and his Lund collaborators have shown how this leads to an extension of the ordinary phase space to one which is fractal in nature and which provides, even in the presence of QCD jet phenomena, a way of maintaining a uniform measure (produced particle density) in the extended phase space. It is the purpose of this paper to elaborate on this approach, using coordinates somewhat different than employed by the Lund group, but which we find more convenient. The main point is simply the suggestion that fractal phase space, using this choice of variables, may be a convenient and practical diagnostic tool in the phenomenological analysis of multiparticle and multijet processes at high energy.

In Section 2, we review the properties of the lego variables η and ϕ. In Section 3, we introduce jets into the lego plot, along with a definition of jets which leads to the extension into fractal phase space. Section 4 is devoted to kinematics, where the same multijet production phenomenology is viewed from a variety of reference frames. Section 5 is devoted to a more geometrical view of extended phase space, using an analogy to plumbing. In Section 6 we extend the picture to include the leading-logarithm multijet description of perturbative QCD. In Section 7, we describe in plumber's language the "color-coherence," or "angular-ordering" effects present in QCD. Section 8 is devoted to an illustration of these ideas using the well-known "string effect" in the processes $e^+e^- \rightarrow q\bar{q}g$ and $e^+e^- \rightarrow q\bar{q}\gamma$. In Section 9, we make a few comments regarding hadron-hadron collisions. Concluding remarks

are contained in Section 10.

2. A Review of Lego Variables

In a high-energy *fixed-target* experiment almost all particles are produced at small angles. If we place a screen transverse to the incident beam direction and downstream of the target, the particle distribution impinging on that screen will be nonuniform. However, if we subdivide it as shown in Fig. 1(a), then within each cell the mean number of particles will be roughly the same. Note that in Fig. 1(a) we have divided the azimuth into *nine* sectors, so that

$$\Delta\phi = 2\pi/9 = 0.698 \approx 0.70 \ . \tag{2.1}$$

Likewise the radial coordinate, essentially θ, is subdivided by factors 2, so that the pseudorapidity η[1]

$$\eta = -\log \tan \theta/2 \tag{2.2}$$

is divided, to excellent accuracy, into subintervals of the same size:

$$\Delta\eta = \log 2 = 0.693 \approx 0.7 \ . \tag{2.3}$$

Actually the mean number of particles per cell as defined here is

$$\langle n \rangle = 0.5 \, \frac{d^2 N}{d\eta \, d\phi} = \frac{0.5}{2\pi} \left(\frac{dN}{d\eta} \right) < 1 \tag{2.4}$$

even at SSC energies.

---

1 We shall not explicitly distinguish the rapidity y from pseudorapidity η in what follows.
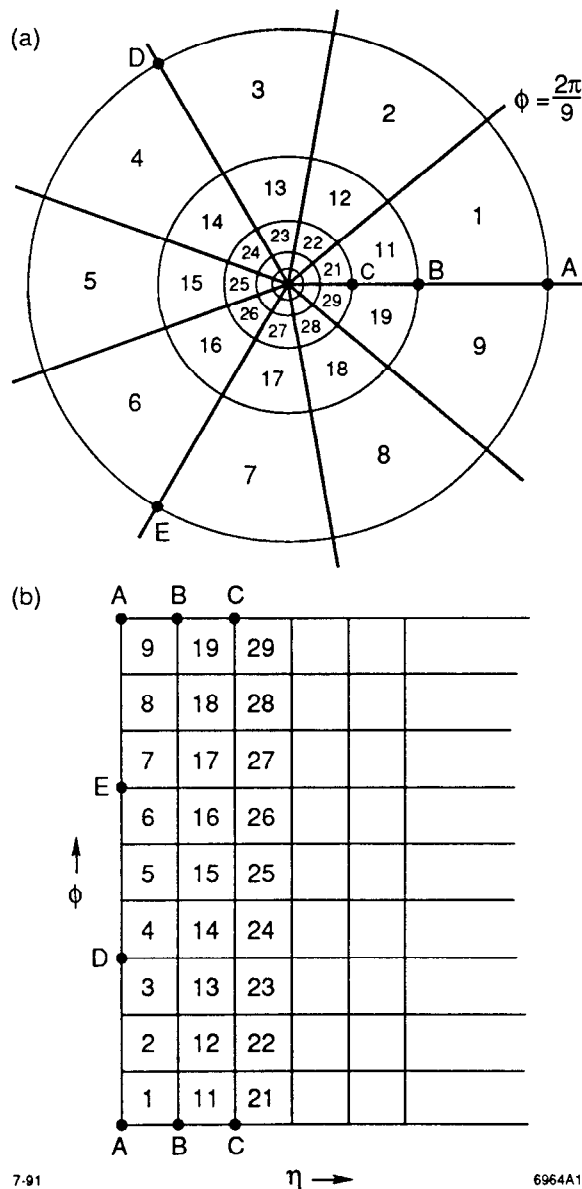
Figure 1. (a) Phase-space as seen in fixed-target geometry. (b) The same phase space as described in the lego variables η and ϕ.

The virtue of the usual lego plot is that it maps this picture into rectangular $\eta - \phi$ coordinates, as shown in Fig. 1(b), because the resultant particle density is approximately uniform when expressed in this way, and the element of area is proportional to the phase-space area.

3. Jets

A jet is a local concentration of produced particles in η, ϕ space with a total transverse-momentum p_t in excess of some minimum value, typically at least a few GeV.

There are a variety of possible algorithms for defining jets, but for our purposes it is convenient [3] to define a jet as *all particles within a circle in the lego plot with radius 0.7, provided the summed p_t within the circle exceeds the threshold value.* To be sure, this algorithm does not state how to precisely choose the center of the circle and how to deal with jets which overlap, *i.e.* jet pairs whose axes are, say, 1 unit of $\eta - \phi$ apart. Both these questions will be addressed later.

With the above definition of a jet, we may expect the population within the circle of radius 0.7 to be nonuniform, and in fact similar to the fixed target population of Fig. 1(a). It is natural, therefore, to introduce polar coordinates within the circle of radius 0.7 [Fig. 2(a)]. And, as before, it is again natural to remap those polar coordinates into rectangular coordinates [Fig. 2(b)]. In this composite phase-space the population of produced particles should be, within statistical fluctuations, fairly uniform—provided there are no additional jets in either the original lego plot or the extension we have created, and provided the p_t of the jet is large enough for a "central plateau" region to exist.

In a normal *pp* collision the area of the lego plot (*i.e.* the region populated by the produced particles in a generic, "minimum-bias" event) is approximately

$$A = 2\pi \log s \; . \tag{3.1}$$

If a pair of jets appear in the final state corresponding to a hard collision with

6
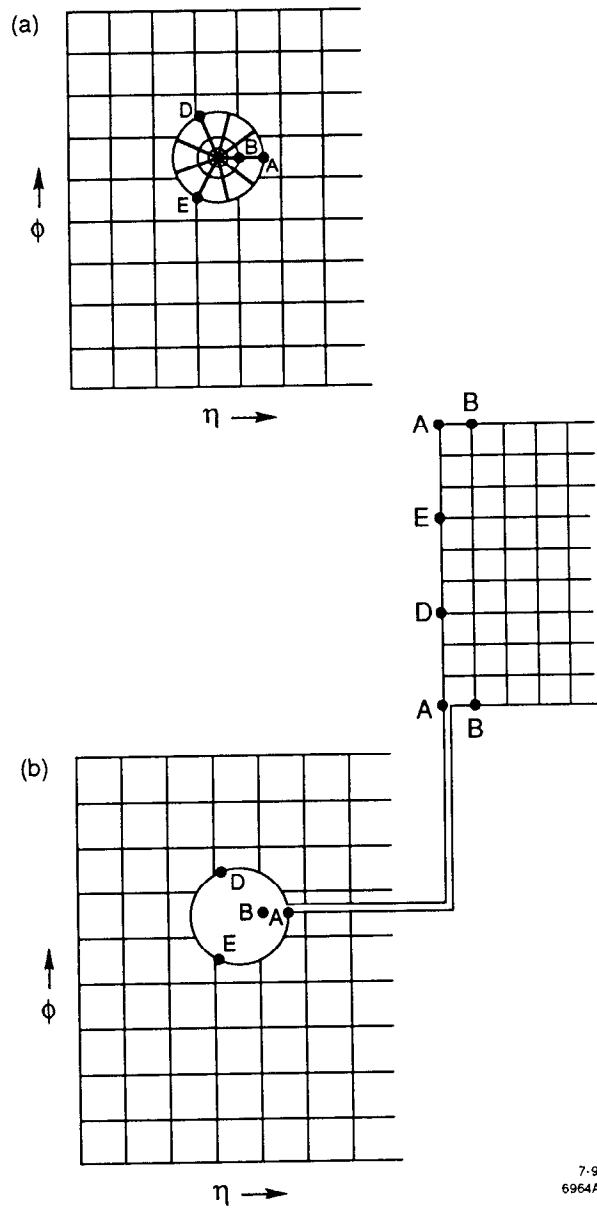
Figure 2. (a) A lego plot within which a jet is found within a circle of radius 0.7, as exhibited. (b) The same lego plot, but with the contents within the circle of radius 0.7 remapped into rectangular lego variables.

momentum transfer p_t, then the area of the extended lego plot is

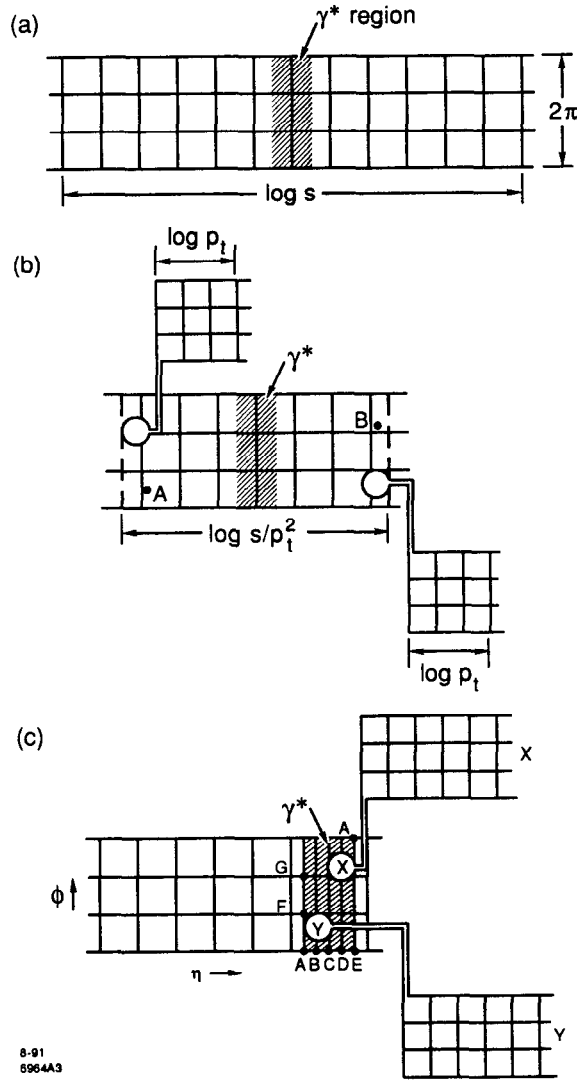$$A' = 2\pi \log s + 2\pi \log p_t^2 \qquad (3.2)$$

7

and the multiplicity of produced particles grows accordingly.

In QCD, extra gluons of lower p_t scales can also be radiated. This provides new populations of jets which again extend the entire lego plot, including the extensions we have exhibited. The self-similar character of this extension should be evident. This gives rise to a phase-space area with a fractal dimension. The total area will depend on the "resolution," *i.e.* the value of minimum p_t chosen. We do not follow the mathematics of this here, much of which can be found in the series of Lund papers [2]. If the minimum p_t scale is chosen to be roughly where ordinary hadronization takes over and below which observable jet structure is at best obscure and at worst nonexistent, then once all jets with p_t exceeding the minimum value have been included, we expect the population of produced particles in the extended phase space so generated to be reasonably smooth.

4. Some Kinematics

Before continuing this discussion, let us review a few kinematic facts of life. These will help in resolving the aforementioned question of separating overlapping jets and of distinguishing those properties of the picture we have introduced which have an invariant meaning from those which depend upon the frame of reference used. These ideas are best exhibited in examples drawn from e^+e^- physics, rather than hadron-hadron collisions. The two points we make, quite elementary, are that a rotation of coordinates can (1) create "kinematic" jets and (2) expand or contract the "size", as seen in the lego plot, of real jets.

We first consider the classic two-jet final state for the process $e^+e^- \to q\bar{q}$, as seen in a variety of coordinate frames.:

(a)

γ^* region

2π

log s

(b)

log p$_t$

γ^*

B

A

log s/p$_t^2$

log p$_t$

(c)

X

γ^*

A

ϕ

G

F

X

Y

η →

A B C D E

Y

8-91
6964A3

Figure 3. (a) The lego plot for a 2-jet $e^+e^- \rightarrow q\bar{q}$ event, with longitudinal coordinates chosen to be the axis of the $q\bar{q}$ jets. Note the new "pixel size" $\Delta\eta = \Delta\phi = 2.1$ (and the impossibly high $\sqrt{s}$ chosen!!). (b) The lego plot for the same process, but viewed in a coordinate system rotated by an angle $\theta \sim 2p_t/\sqrt{s} \ll 1$. (c) The same 2-jet event but with a "typical" production angle $\theta \sim 1$. The distribution has been boosted along the z-axis in preparation for another rotation of coordinates.

In Fig. 3(a), the $q\bar{q}$ jet axes are along the longitudinal direction, and we obtain the standard lego plot, with a more-or-less uniform particle distribution within. Note that we distinguish the cms frame of the parent virtual photon by shading the region of the phase space for which the produced particles have low, sub-GeV,

9

momentum in that frame. This has an invariant meaning, and can be useful in more complicated situations to be described in what follows.

In Fig. 3(b), we have rotated coordinates by an angle

$$\theta = \frac{2p_t}{\sqrt{s}} \ll 1 \qquad (4.1)$$

and we see two "jets" at the edge of the longitudinal phase space. Note that the longitudinal phase space has shrunk from an original length $\ell \sim \log s$ to a new length

$$\ell \sim \log s - 2 \log p_t . \qquad (4.2)$$

This is compensated by the phase space, $\sim 2 \log p_t$, contained within the jets (circles of radius 0.7). This differs from the examples given in Section 3, which extended the total phase-space area. Here a coordinate-rotation should not (and does not) affect the physics.

It is interesting that if one draws, as shown, tangents to the circles of radius 0.7, they serve as a quite practical definition of the boundary of the phase space. That is, if one estimates (Appendix 1) the mean number of particles $\langle n \rangle$ leaking to the outside, the answer is

$$\langle n \rangle = \frac{1}{2} e^{-2R} \left(\frac{dN}{d\eta} \right) = \frac{1}{8} \left(\frac{dN}{d\eta} \right) \qquad (4.3)$$

where $R = 0.7$ is the radius of the circle defining the jet, and $dN/d\eta$ is evaluated for the rapidity at the center of the circle; in our case $\eta \approx \log \sqrt{s}/p_t$.

Evidently if there is a stray particle on the outside, it will preferentially be found at an azimuthal angle ϕ near that of the "jet." Likewise there will be a

depletion within the "allowed" phase space in the azimuthal directions opposite to those of the jets [points A and B in Fig. 3(b)]. This will be discussed further in the context of the "string-effect" in Section 8.

In Fig. 3(c), we have rotated coordinates further to a "typical" value, so that the separation $\Delta\eta$ of the two jets is $\lesssim 2$ units. We have also boosted the configuration along the z axis into a "fixed-target" geometry–although this change is not very noticeable at this point, due to the simple transformation properties of the lego variables under the boost.

However, having made the boost, we again consider a rotation of coordinates. The effect is best seen by first mapping the distribution into polar coordinates [Fig. 4(a)] and then making a small rotation—which simply amounts to a translation of axes in Fig. 4(a).

Once the translation has been made [Figs. 4(b), 4(c)], polar coordinates may be re-introduced and the map to lego variables performed. Depending upon the magnitude of the rotation, we may end up again with a two-jet configuration, overlapping jets [Fig. 5(a)], or a single jet [Fig. 5(b)]. This latter configuration is what one would expect if one had fixed target kinematics (positrons incident on atomic electrons) and a stupid choice of z-axis, $i.e.$ one not along the beam direction.

The example of overlapping jets in Fig. 5(a) is especially instructive. It shows that even when jet products overlap in the lego plot they need not overlap intrinsically (although they occasionally will). And a way to resolve the ambiguity when it occurs is to first make an appropriate longitudinal boost and to then make a simple, small *rotation* of coordinates. The best choice is probably to rotate in such a way that both jets shrink into a common circle-of-radius 0.7. Then, upon remapping
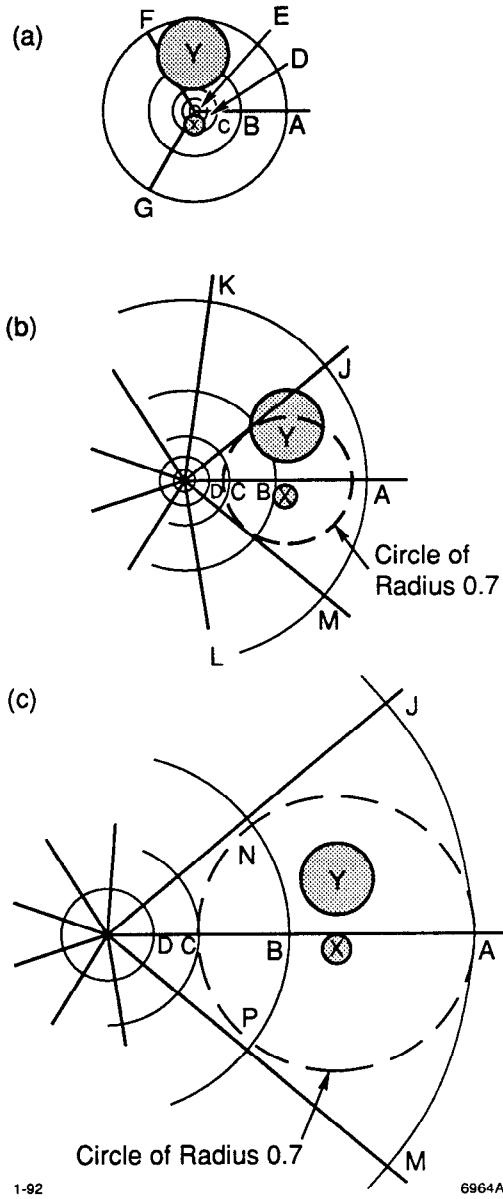
11

Figure 4. (a) The lego plot of Fig. 3(c) remapped into fixed-target polar coordinates. (b) The polar plot of Fig. 4(a) after a rotation of coordinates. The rotation angle is such that the jets X and Y overlap, *i.e.* have a separation of order 1. Notice that the circles defining the jet region have shrunk. (c) The same polar plot, but with a larger rotation angle, such that both jets X and Y shrink into a single circle-of-radius 0.7.
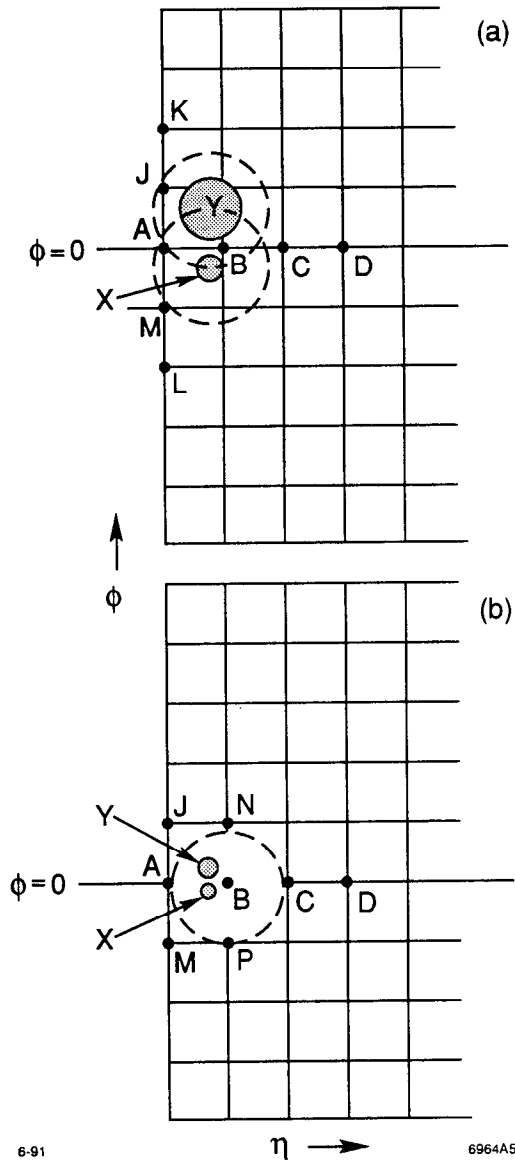
12

Figure 5. (a) The polar plot of Fig. 4(b) remapped into lego variables. The dashed lines show circles-of-radius 0.7 drawn around the jet cores X and Y, which have shrunk as a consequence of the coordinate-rotation. The circles of-radius 0.7 overlap, a situation best avoided by an additional coordinate rotation. Note we have chosen $\phi = 0$ at the center of the lego-plot in order to better display the jets. (b) The polar plot of Fig. 4(c) remapped into lego variables. Essentially all collision products are now found within the circle-of-radius 0.7 shown.

the contents into lego variables, the two jets will in most cases be resolved.[2]

---

2 Another way is simply to choose a circle of radius $R > 0.7$ sufficient to contain all jet products, and then remap to polar coordinates. I am not sure which choice is to be preferred.

We also mention here a way of resolving the issue of how best to center the circle-of-radius-0.7 surrounding a jet core. If the contents of the circle, when expressed in lego variables, have a leading "kinematic jet" [Fig. 3(b)], then the center has been chosen unwisely. Any choice that does remove the leading "kinematic jet" [Fig. 3(a)] may be deemed acceptable; *i.e.* the variation in such choices may be a measure of the intrinsic uncertainty in determining the coordinates of the initiating parton.

5. Plumbing

The lego-surface is periodic in ϕ, so that it really is the surface of a cylinder; *i.e.* a pipe. From this point of view the addition of extra QCD jets to a collinear two-jet lego plot, as in Fig. 3, simply amounts to cutting holes of radius 0.7 in the pipe (which has in these units radius 1) and attaching new pipes to it, each of length $\log p_t$ (Fig. 6). Likewise the "kinematic jets" correspond to "elbows"—$90°$ bends—in the pipe (Fig. 7). This collection of plumber's fittings can be augmented by "caps," representing the leading-particle regions of phase-space at the ends of the lego plot, regions which arguably ought to be left in polar coordinates rather than being mapped into lego-variables (Fig. 8).

We now see that changes of coordinate systems can create or move elbows in sections of pipe, without significantly changing their overall length, something which, as mentioned in Section 4, is an intrinsic property. "Tees" and caps are likewise intrinsic properties of the event as well. A "tee" represents a vertex where a gluon was emitted, so it is labeled by an $\alpha_s(p_t^2)$, with a reasonable estimate of $\log p_t$ being the length of the shortest section of pipe emergent from the tee.
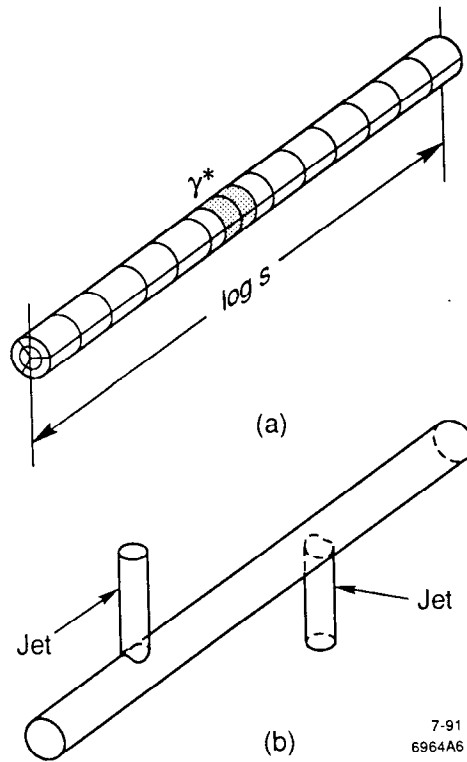
Figure 6. (a) The lego plot of Fig. 3(a) rolled up into a cylinder, or "pipe." (b) A 2-jet event; the jet products are found on the surfaces of the new pipe segments.

One other type of plumber's fitting, a connection or sleeve, is appropriate for marking a specific region on a pipe (piece of lego plot). We encountered already such a case in $e^+e^- \rightarrow q\bar{q}$, where the shaded rapidity region (Fig. 3), which exhibits the frame in which the initial state virtual photon is at rest, is an intrinsic property of the event structure and is useful to mark.

There evidently are also generalized "tees" corresponding to vertices where two or more gluon jets emerge form the same region of phase space. These are relatively rare and will be neglected in what follows.
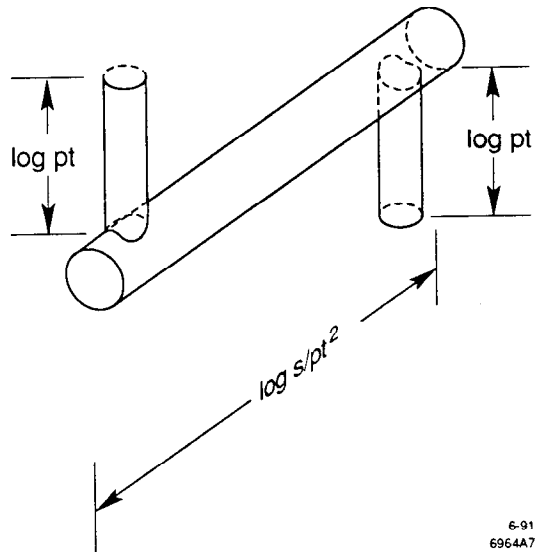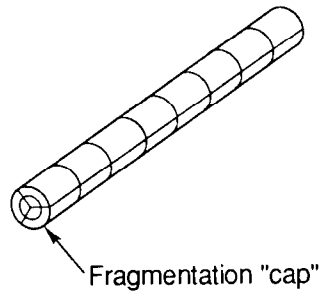
Figure 7. A plumber's view of the "kinematic jets" of Fig. 3(b), generated by a small coordinate rotation from Fig. 6(a) [or 3(a)].
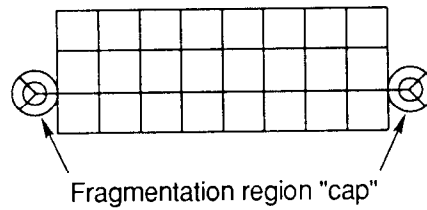
Figure 8. (a) "Caps" attached to the ends of the lego plot, intended to cover the leading-particle, fragmentation region. (b) A plumber's view of Fig. 8(a).

16

6. QCD Leading Logs: Decorating the Plumbing

For a given event, the basic architecture will be defined by the configuration of the highest-p_t jets, *i.e.* the pieces of pipe of greatest length. The generic $e^+e^- \to q\bar{q}$ event we discussed has two pieces of pipe of length $\log \sqrt{s}$, connected by a γ^* (or Z) "sleeve," which marks the e^+e^- cms frame.
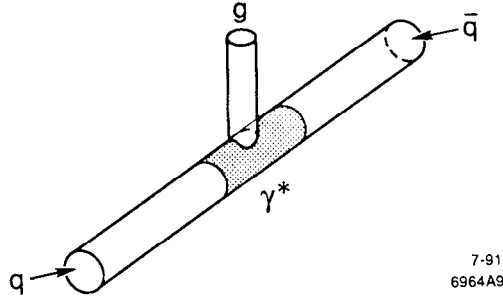

Figure 9. A plumber's view of a "Mercedes" 3-jet final state in $e^+e^- \to q\bar{q}g$.

In most cases no additional QCD jet will have $p_t \sim \sqrt{s}$. But occasionally there will be "Mercedes" 3-jet events, where the junction "tee" occurs at the γ^* "sleeve" (Fig. 9). But whatever the structure at the highest p_t scale is, we may then expect a "decoration" of the basic structure from lower-p_t gluon (or $q\bar{q}$) jets. The probability per unit rapidity of finding an extra jet of scale p_t attached to a quark line is [4] , in "leading log" approximation

$$\frac{dP}{d\eta} \simeq \frac{3\alpha_s(p_t^2)}{2\pi} \int \frac{dp_t^2}{p_t^2} .$$ (6.1)

So until the scale is quite low, not too many will occur.

One must "decorate" from the highest p_t scales to the lowest. That is, one breaks up the p_t range into intervals. Starting with the highest p_t which is relevant,

one appends the pieces of pipe of length $\log p_t$. Then one goes down in scale and adds the shorter lengths to the *entire* structure. As already mentioned in Section 2, this will generate an architecture for this plumbing which is fractal. The procedure will terminate (as far as perturbative QCD is concerned) when the pipes to be added have no significant length, but are all cap. At the lowest p_t scale, one then has to somehow address the physics of hadronization. The net result, however, should be a quite uniform distribution of particles over the entire structure of plumbing generated perturbatively.

7. QCD Coherence Effects: Coloring the Plumbing

Amplitudes for radiation of QCD jets must obey the rules of "color-coherence," or "angle-ordering" [5] , and it is appropriate here to describe (without derivation) what it means in this language. We consider for definiteness the process $e^+ e^- \rightarrow q\bar{q}$ + gluons. Suppose there are two additional highest-p_t gluons, so that the lego plot is as in Fig. 10(a), and the corresponding plumbing as in Fig. 10(b). The problem we consider is how the amplitudes for subleading jets of lower p_t are to be computed. To answer that first requires attaching color labels to the quarks and gluons (Fig. 11). Once this is done, the radiation of the subleading gluons is to be calculated by considering the soft, subleading gluon emission from each individual color line as if it were a $q\bar{q}$ pair. What this means in terms of the lego plot variables is that the distribution of radiated gluons is an incoherent sum (to leading order in N_c, the number of colors) of contributions from distinct subregions of the lego plot. In our example, there are three such regions, as shown in Fig. 12. The radiation from color-line A fills the region A shown in Fig. 12(a), in a manner identical to gluon emission from a $q\bar{q}$ pair creating the two-jet configuration shown
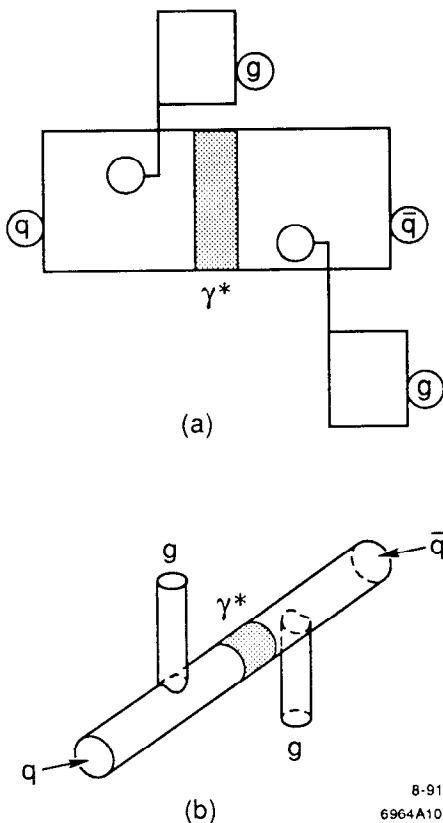
18

Figure 10. (a) Extended lego plot for the process $e^+e^- \to q\bar{q}gg$. (b) The plumber's view of Fig. 10(a).

as shaded. In a similar way, the regions B and C of the lego plot are populated from the radiation from lines B and C. We see that the gluon jets get twice the radiation, because gluons have two color labels, not one. (Actually, the ratio should be $2N_c^2/(N_c^2 - 1) = 9/4$ when the color factors are computed more carefully.) In fact it is sometimes convenient to think of the gluon lego plot as double-sided [6] , with each side labeled by one of its color indices. Then half of the subleading jets emerge from the back side, the other half from the front. However, for quark jets there is only one color index, hence only one distinguishable side.

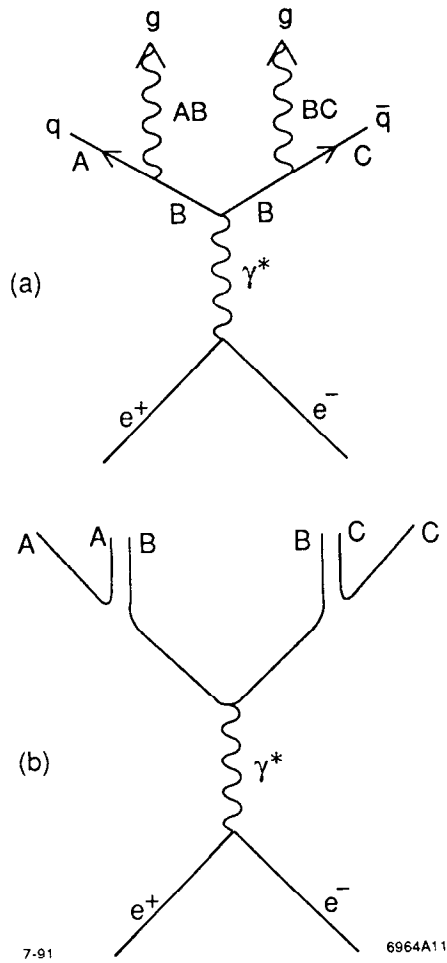In terms of plumbing, this picture translates simply into "painting" the appro-

Figure 11. (a) Feynman diagram for the process $e^+e^- \rightarrow q\bar{q}gg$, with color labels attached to the lines. (b) Schematic of the color flow.

priate surfaces of the pipes with the appropriate color, A, B, ..., in accordance with the amplitude for the process. Emission of subleading jets from these surfaces is then an incoherent sum of gluon emissions from each section of plumbing labeled by a given color index. Since any such subsystem is essentially a set of pipe segments connected effectively by elbows, an easy way to determine the gluon radiation from a given subsystem is to carry out a sequence of Lorentz-boosts which straighten out the bends in that subsystem, leaving effectively a straight section of
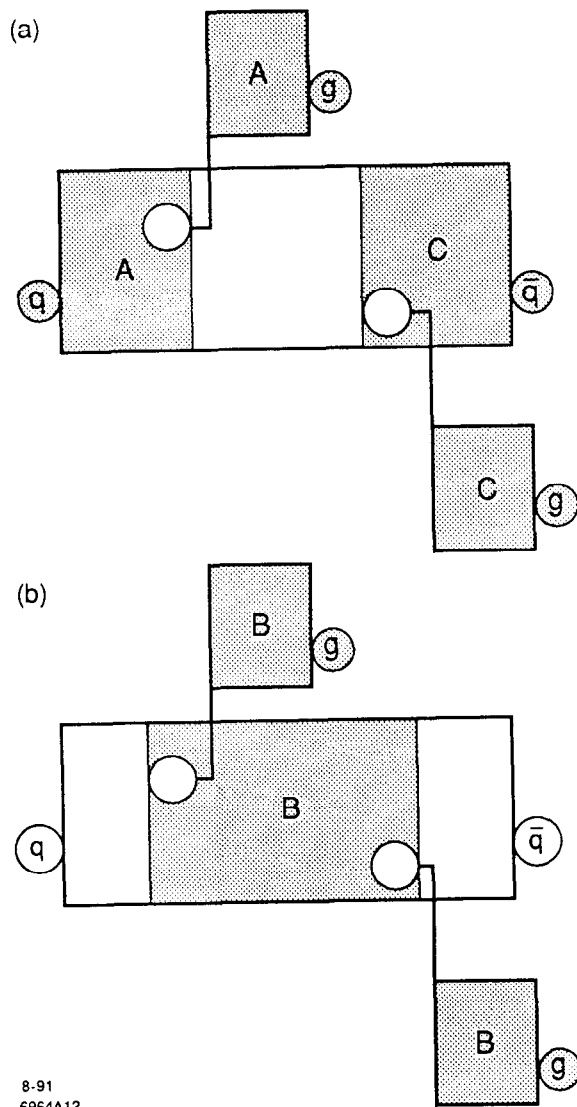
Figure 12. (a) Regions of phase space for which subleading gluons may be emitted from the leading quark lines. (b) Region of phase space from which subleading gluons can be radiated from the virtual quarks produced by the γ^*.

pipe. The decoration of subleading jets onto that subsystem is identical to decorating subleading gluons onto a collinear $q\bar{q}$ pair. [Of course once such a subleading gluon is radiated, the lego surface must be "repainted" appropriately.]

There is, to be sure, some ambiguity on how to decorate elbows and tees. But

probably the most consistent rule is to perform the decoration of a subsystem in its collinear reference frame as suggested above (*i.e.* in a frame where the plumbing painted with the subsystem color index is a straight pipe). We shall give an example of how this works in Section 8, where the "string effect" in 3-jet production is discussed.

In all this discussion, we again emphasize that the decoration process must proceed from high-p_t jets to low, so that the full fractal structure of the phase space is created. Because of the running of α_s, it is mainly low-p_t minijets which will be the predominant feature generated by this process.

8. An Example: The "String Effect" in $e^+e^- \to 3$ Jets

The processes $e^+e^- \to q\bar{q}g$ and $e^+e^- \to q\bar{q}\gamma$ have provided a classic example of QCD coherence effects. [7] . We here review the phenomenon in qualitative terms from our point of view. What we will compare is the particle density emitted opposite to each of the jets. This can be defined in a precise way, by specifying in all cases a reference frame in which the remaining two jets are collinear.

Start with the process $e^+e^- \to q\bar{q}\gamma$ and first estimate the particle production opposite the γ. The lego-plot is shown in Fig. 13 and the particle density is to be computed at point A. Clearly this is just $d^2N/d\eta\,d\phi$ for an ordinary $e^+e^- \to q\bar{q}$ event.

More interesting is to compute the density opposite the q jet in the frame in which γ and $\bar{q}$ are collinear. The lego plot is shown in Fig. 14, and the plumbing is essentially an "elbow" as far as hadron emission is concerned, since we have just boosted the uniform two-jet distribution seen in Fig. 13 to a different Lorentz frame.
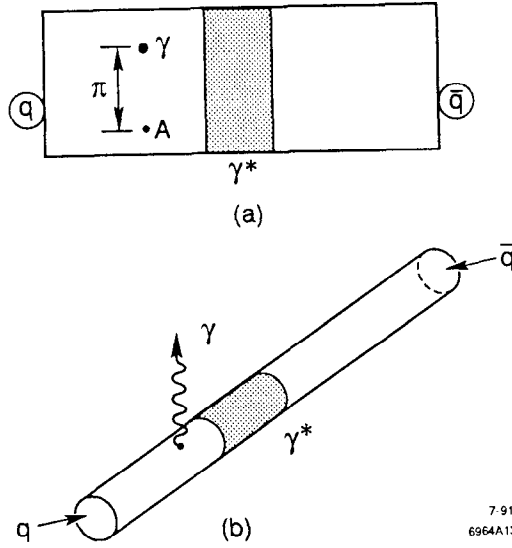
Figure 13. (a) Lego plot for the process $e^+e^- \to q\bar{q}\gamma$ in a reference frame in which the $q\bar{q}$ pair is collinear. (b) A plumber's view of Fig. 13(a).

To estimate the density at the base of the "elbow," point B, it is convenient to boost to a fixed target frame of reference and remap the configuration in polar coordinates (Fig. 15). The density at point B is just what one gets by extending the lego variables centered around the q jet core into the remainder of the phase space, since in this frame there is just a collinear jet configuration with axis in that direction. What now needs to be done is to compare in the neighborhood of point B this measure with the lego-plot measure centered about the γ-$\bar{q}$ jet axis. This is just the area of the shaded sector versus the area of the cross-hatched one. The ratio is about $1/4$. Hence we conclude that the particle density opposite the q jet (in this collinear frame) is about 25% of the density opposite the photon jet (in the $q\bar{q}$ collinear frame). In passing we note that the density expected in the "forbidden" region of the lego plot, *i.e.* the region to the left of the tangent CD in Fig. 14(a) is quite small since it corresponds to the region interior to the circle CDE in Fig. 15, which covers only 50% of a unit of $\Delta\eta\,\Delta\phi$ as measured from the
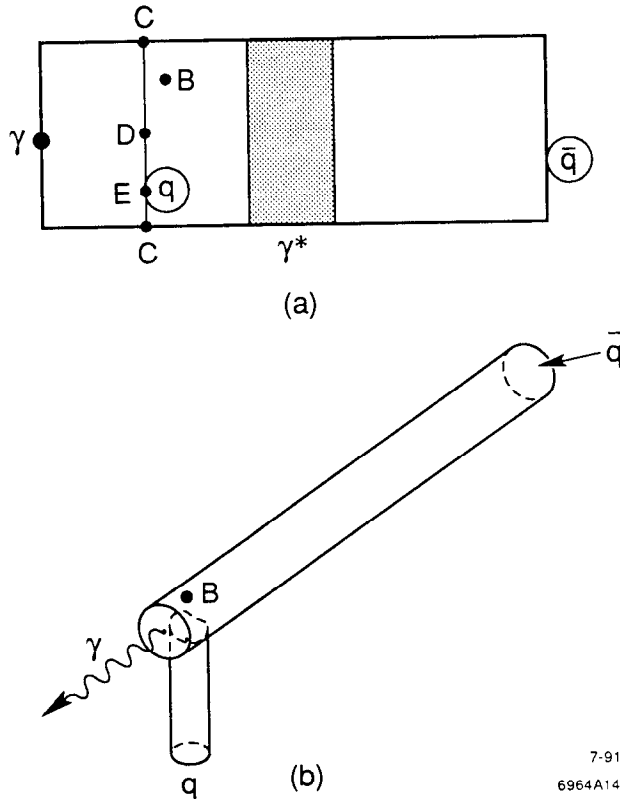
Figure 14. (a) The lego plot for $e^+e^- \to q\bar{q}\gamma$ in a reference frame in which the $\gamma\bar{q}$ pair is collinear. (b) A plumber's view of Fig. 14(a).

q-jet axis. This qualitative result is made more quantitative in the appendix.

It is now straightforward to consider the process $e^+e^- \to q\bar{q}g$. Given the color labeling shown in the Feynman diagram in Fig. 16, we paint the surfaces of the lego-plumbing as shown in Fig. 17. Figure 17(a) is appropriate to consideration of the particle density opposite the gluon jet where we see [Fig. 18(a)] a net depletion of $\sim 50\%$ relative to the densities in the rest of the $q\bar{q}$ jets. In Fig. 17(b), however, where the kinematics is appropriate to the distribution opposite the $\bar{q}$ (or q) jet we see an enhancement of 25% relative to what is expected in the quark jet. This is the "string effect," expected theoretically and seen experimentally.
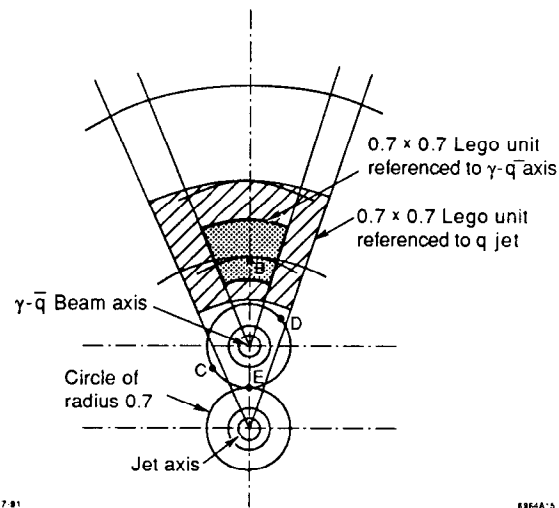
24

0.7 × 0.7 Lego unit
referenced to γ-q̄ axis

0.7 × 0.7 Lego unit
referenced to q jet

γ-q̄ Beam axis

Circle of
radius 0.7

Jet axis

Figure 15. The lego plot of Fig. 14 remapped into polar coordinates after a large boost in the z-direction.
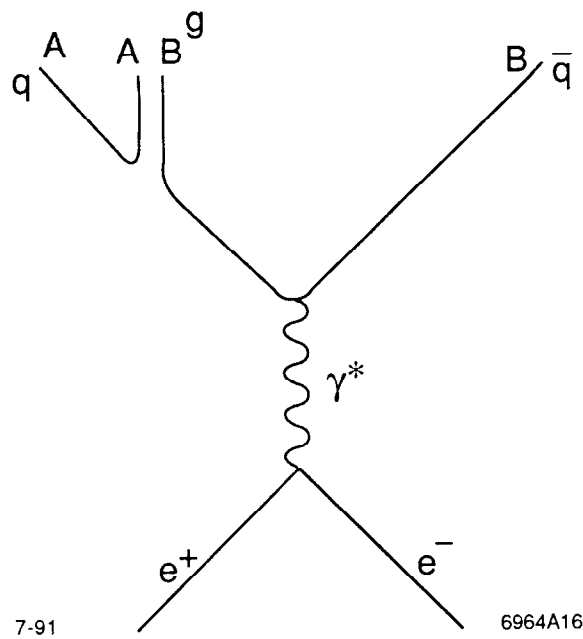

Figure 16. Color labels for the process $e^+e^- \rightarrow q\bar{q}g$.

9. Hadron-Hadron Collisions: "Hole Fragmentation"

In hadron-hadron collisions there is always the preferred axis of the incident beams which provides the natural coordinate system for laying out the lego vari-
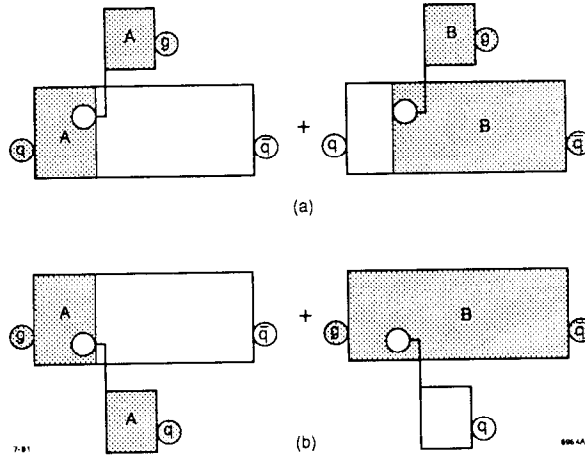
25

Figure 17. (a) Color flow in the lego plot for the process $e^+e^- \to q\bar{q}g$ in a collinear $q\bar{q}$ frame. (b) Color flow in the lego plot for the process $e^+e^- \to q\bar{q}g$ in a collinear $g\bar{q}$ frame.

ables. In general, the analysis parallels what we have already discussed. Here we only mention one additional feature, of importance because the initial-state partons responsible for the hard collisions carry color. Initial-state color leads to initial-state gluon radiation, and it is appropriate to describe its properties in the language we have introduced. Suppose for definiteness the process is $gg \to ggg$, with color indices labeled as shown in Fig. 19. The incident initial-state gluons are usually specified to have a definite longitudinal momentum $p_\ell = xp_{\text{beam}}$, and a "small," usually unspecified, transverse momentum p_t. Once the p_t is specified, say 0.7 GeV within a factor two, the initial-state rapidities of the incident gluons can be estimated within an uncertainty of order $\pm$ 0.7. We mark these regions of the phase-space as "hole-fragmentation" regions, since in the collision those initial-state partons are abruptly transported to some distant region of phase space, thereby requiring some special final-state hadronization to occur in their original region of phase space [8] .

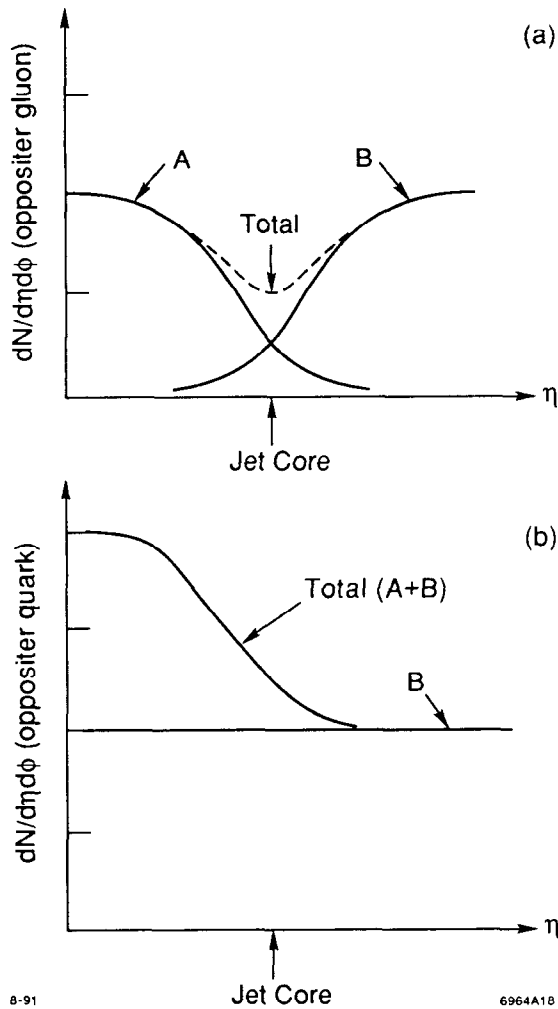The "color-dipole" rules of leading-log perturbative QCD may now be applied

Figure 18. (a) Rapidity distribution of particles produced opposite the gluon jet in $e^+e^- \to q\bar{q}g$, as seen in a collinear $q\bar{q}$ reference frame. (b) Rapidity distribution of particles produced opposite a $\bar{q}$ jet in $e^+e^- \to q\bar{q}g$, as seen in a collinear gq reference frame.

in a straightforward way. The extended lego plot is shown in Fig. 20, with the rules for coloring the surfaces shown. Then the process of decoration of the phase space with softer jets, minijets, and hadrons, as described in previous sections may proceed as before.

In a high-p_t binary gluon-gluon collision, there is predicted to be considerable extra multiplicity along the beam-jet directions, extending out to—but not
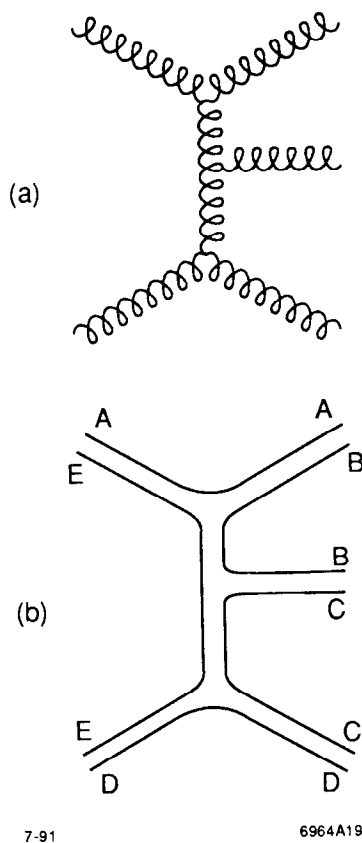
27

Figure 19. Feynman diagram (a) and a choice of color indices (b) for the process $gg \rightarrow ggg$.

beyond—the hole fragmentation regions. It would be interesting to see how sharply this effect is seen experimentally, and whether it is sharp enough to distinguish initial-state quarks from initial-state gluons.

The concepts of hole fragmentation also apply to lepton-hadron collisions; the rules for color flow in this case are similar and are left to the interested reader.
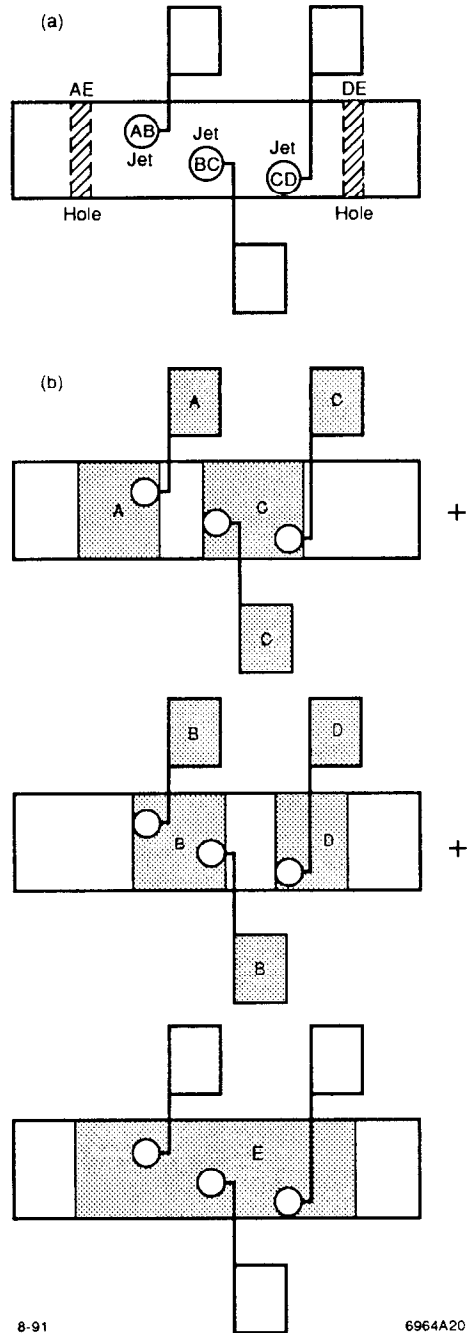
Figure 20. (a) Lego plot for $gg \rightarrow ggg$. The "hole" fragmentation regions mark the estimated rapidities of the initial-state gluons. (b) Rules for "coloring" the lego plot for determining emission of subleading gluons, in accordance with the choice of color indices shown in Fig. 19(b).

10. Conclusions

Of what use is all this? We believe that the variables we have used are a practical tool for describing complex event structures containing jets in terms of (fractal) extensions of the phase space, and also that the definition of jet that is used is sufficiently precise to be a very practical one. The problem of distinguishing distinct jets which overlap when viewed in the usual lego variables may be resolvable using the flexibility in choosing coordinates, as described in Section 4. The description appears to be eminently suited for visual computer displays of event structure, and we hope that someone expert in software development might pick this idea up.

Important here is our emphasis on individual particles, and not on transverse-momentum flow. There is a need to display distributions of "entropy" (particle-numbers) as well as "energy" (transverse-momenta); these are complementary concepts. Also noteworthy is the need for very good resolution in $\Delta\eta$ and $\Delta\phi$ of individual hadrons (and photons) in order to delineate accurately the populations in the extended phase space.

This work was stimulated in large part [9] by consideration of the physics associated with a full-acceptance detector for SSC-scale proton-proton collisions. A prime goal of such a detector, or any other having broad rapidity acceptance, should be the perception and classification of patterns or morphologies of individual events which have considerable complexity. One's choice of coordinates or descriptive elements is for such applications crucial. We believe the choice made here has much virtue and is worth pursuing.

APPENDIX

Consider the process $e^+e^- \rightarrow q\bar{q}$, with the jets produced at a small angle θ relative to the e^+e^- collision axis:

$$\theta = \frac{2p_t}{\sqrt{s}} \ll 1 \, . \qquad\qquad (A.1)$$

Define the "kinematic jets" as the contents of the circle of radius 0.7 surrounding the jet axes as seen in the lego-plot referenced to the e^+e^- beam directions. Then draw tangents in the lego plot to those circles as shown in Fig. 3(b) [the dashed lines]. We are interested here in how many produced particles leak to the region exterior to the phase space bounded by those tangents. We assume $p_t \gg 1\ GeV$ and also assume, in a frame of reference with z axis aligned along the jets, that the relevant secondary hadrons are produced with a flat rapidity distribution. However we work hereafter in the frame referenced to the e^+e^- beam directions.

The four-momentum of the primary quark is

$$p_\mu \cong \left(\frac{\sqrt{s}}{2}, \, \frac{\sqrt{s}}{2} - \frac{p_t^2}{\sqrt{s}}, \, \overrightarrow{p_t} \right) \qquad\qquad (A.2)$$

and the four-momentum of a secondary hadron will be

$$\ell_\mu \cong z p_\mu + (k_t)_\mu \qquad\qquad (A.3)$$

with

$$k_t^\mu = \left(0, \Delta k, \overrightarrow{k_t} \right) \qquad\qquad (A.4)$$

expected to be on average no more than 1 GeV. The longitudinal momentum Δk is chosen such that $\ell^2 = 0$. What we really need are the rapidities of primary quark

31

and secondary hadron, which are

$$\eta_{\text{quark}} = \frac{1}{2} \, \ell n \, \frac{p_0 + p_z}{p_0 - p_z} = \ell n \, \frac{\sqrt{s}}{p_t}$$

$$\eta_{\text{hadron}} \cong \frac{1}{2} \, \ell n \, \frac{\ell_0 + \ell_z}{\ell_0 - \ell_z} = \ell n \, \frac{(\ell_0 + \ell_z)}{|\vec{\ell_t}|} = \ell n \, \frac{z\sqrt{s}}{|z\vec{p_t} + \vec{k_t}|} \, . \tag{A.5}$$

In order that the hadron rapidity exceed the jet rapidity by an amount R (the radius of the circle defining the jet contents: $R = 0.7$), we must have

$$(\eta_{\text{hadron}} - \eta_{\text{jet}}) = \ell n \, \frac{|z\vec{p_t}|}{|z\vec{p_t} + \vec{k_t}|} > R \tag{A.6}$$

or

$$\frac{|z\vec{p_t} + \vec{k_t}|}{|z\vec{p_t}|} < e^{-R} \, . \tag{A.7}$$

The condition in Eq. (A.7) can only be satisfied if

$$1 - e^{-R} < \frac{|\vec{k_t}|}{|z\vec{p_t}|} < 1 + e^{-R} \tag{A.8}$$

and only then for a limited set of relative orientations. For a given magnitude of

32

k_t and z, the geometry is shown in Fig. 21. We see that the azimuthal angle ϕ
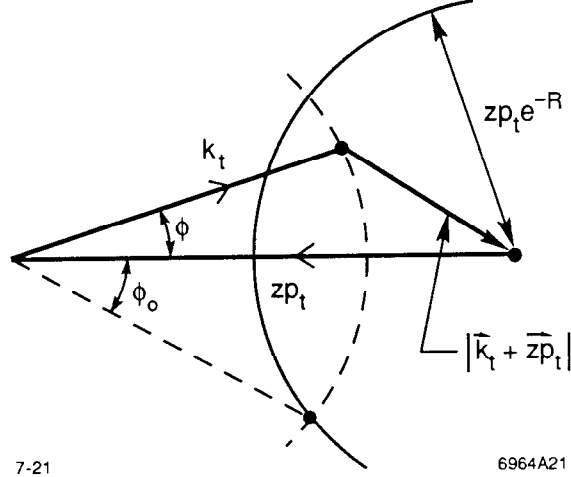

Figure 21. Geometry for the calculation of leakage into the rapidity-gap.

must be less than a value ϕ_0 which, to reasonable approximation, is given by the expression

$$\phi_0^2 = \frac{\left(z|\vec{p_t}|e^{-R}\right)^2 - \left(z|\vec{p_t}| - |\vec{k_t}|\right)^2}{|z\vec{p_t}|\,|\vec{k_t}|}\,. \tag{A.9}$$

For fixed $|\vec{k_t}|$ we may therefore estimate the "leakage" ΔN to be

$$\Delta N = \left(\frac{dN}{d\eta}\right) \int \frac{dz}{z} \cdot \frac{2\phi_0}{2\pi} = \frac{1}{\pi}\left(\frac{dN}{d\eta}\right) \int \frac{dz}{z} \sqrt{\frac{z^2 e^{-2R} - (z-x)^2}{zx}}$$

$$= \frac{1}{\pi}\left(\frac{dN}{d\eta}\right) \int \frac{dy}{y^{3/2}} \sqrt{y^2 e^{-2R} - (y-1)^2} \tag{A.10}$$

Here $x = |\vec{k_t}|/|\vec{p_t}|$, and the integration only goes over values of the variable for which the square root is positive. Since k_t disappears from the estimate, we may

33

average over all values of k_t. Finally, in the limit of large R the formula simplifies with the substitution $y = 1 + we^{-R}$. The result is, approximately,

$$\Delta N \cong \frac{1}{\pi} \left(\frac{dN}{d\eta}\right) e^{-2R} \int_{-1}^{1} dw \sqrt{1 - w^2} = \frac{1}{2} \left(\frac{dN}{d\eta}\right) e^{-2R} \qquad (A.11)$$

which is what was quoted in Eq. (4.3).

A more complete analysis is straightforward, but is best done directly via Monte Carlo simulations.

REFERENCES

[1] For a good review, see H. Harari, *Proceedings of the 14th Scottish Universities Summer School in Physics* (1973), ed. R. Crawford and R. Jennings, Academic Press (N.Y.), 1974, p. 297.

[2] B. Andersson, P. Dahlqvist, and G. Gustafsson, Phys. Letts. B214, 604 (1988). A recent discussion is given by G. Gustafsson, Lund preprint, LU TP 90-16 (November 1990).

[3] Essentially this definition is advocated by J. Huth *et al.*, Fermilab preprint FERMILAB-CONF 90-249-E.

[4] See for example Ref. 2 for more details.

[5] Y. Azimov, Yu. Dokshitzer, V. Khoze, and S. Troyan, Phys. Lett. B165, 147 (1985).

[6] This idea goes back to G. Veneziano, Nuovo Cimento 57A, 190 (1968).

[7] For reviews see G. Gustafsson, Lund preprint LU TP 90-17 (November 1990), and V. Khoze, CERN preprint CERN-TH 5849 (September 1990).

[8] J. Bjorken, Phys. Rev. D7, 2747 (1973). See also J. Bjorken, Journal de Physique C1, Suppl. 10, Vol. 34, 385 (1973).

[9] J. Bjorken, Expresion of interest to the SSC (EoI-19), SLAC-PUB-5545, to be published in the *Proceedings of the Sixth J. A. Suieca Summer School: Particles and Fields*, Campos do Jordao, Brazil (January 1991), ed. O. Eboli.